Manuscript number XXXXX: IEEE Transactions on Geoscience and Remote Sensing

Multi-Satellite Altimetry Calibration and Validation Using a GNSS Wave Glider in the North Sea

Nigel T. Penna, Philip Moore, Miguel A. Morales Maqueda, Ian Martin,
Paolo Cipollini, Jing Guo, Peter R. Foden, and David E. Gregg

***Abstract*—The concept of in-situ multi-satellite altimetry calibration and validation in the absolute sense using ocean autonomous surface vehicles as GNSS platforms is demonstrated through an experiment in the North Sea during 2016. A Wave Glider equipped with geodetic GNSS travelled to locations ranging from 21 to 78 km from the coast to be directly under four Jason-series tracks and two CryoSat-2 tracks. 5-Hz sea surface heights were estimated from precise point positioning mode processing of GPS+GLONASS data, together with hourly zenith wet tropospheric delays, and used as reference values for altimetry satellite measured sea surface height, tropospheric delay and significant wave height. Sea surface height biases obtained were −30 to −8 mm for Jason-2 using GDR-D products, −40 to +1 mm for Jason-3 using GDR-F products, and −29 mm and +18 mm for CryoSat-2 using SAR mode GOP baseline C products. These biases are almost commensurate with results from previous studies in other regions which used GNSS buoys or onshore GNSS reference stations with geoid and tide extrapolation. The Jason-2 and Jason-3 microwave radiometer-measured zenith wet tropospheric delays differed respectively by −15 mm and −10 mm on average from those measured by the GNSS Wave Glider. Root mean square significant wave height differences of 2-6 cm were obtained between Jason-2/3 and the co-located GNSS Wave Glider, and equivalent differences of 19-21 cm for CryoSat-2.**

***Index Terms*—GNSS Wave Glider, satellite altimetry cal/val, sea surface height, significant wave height, tropospheric delay.**

Manuscript received xxxxxx xx, 2023; revised xxxxxx xx, 202x; accepted xxxxxx xx, 202x. This work was supported by UK Natural Environment Research Council grants NE/K005944/1, NE/K005421/1 and NE/K0054212/2. *(Corresponding author: Nigel T. Penna.)*

Nigel T. Penna, Philip Moore, Ian Martin and David E. Gregg are with the School of Engineering, Newcastle University, Newcastle upon Tyne, NE1 7RU, UK (email: nigel.penna@newcastle.ac.uk).

Miguel A. Morales Maqueda is with the School of Natural and Environmental Sciences, Newcastle University, Newcastle upon Tyne, NE1 7RU, UK.

Paolo Cipollini is with the European Space Agency, Noordwijk-Binnen, South Holland, The Netherlands.

Jing Guo is with the GNSS Research Center, Wuhan University, Wuhan, China.

Peter R. Foden is with the National Oceanography Centre (Liverpool), Liverpool, L3 5DA, UK.

This article has supplementary material provided by the authors and available at https://doi.org/10.1109/TGRS.

I. INTRODUCTION

SATELLITE altimetry measurements are fundamental for determining estimates of sea surface height (SSH), including the wave field, global and regional changes in mean sea level, and provide key input data for validation of, and assimilation into global and regional models of ocean circulation, tides, the sea surface and dynamic topography. The ERS-1 (1991-2000) and TOPEX/Poseidon (T-P) (1992-2000) missions were the first to provide all the instrumentation to precisely measure global mean sea level change from satellite altimetry. The ERS-1 35-day orbit was continued by ERS-2 (1995-2010) and Envisat (2002-2012), while the near 10-day repeat orbit of T-P was continued through the Jason-1 (2001-2013), OSTM/Jason-2 (2008-2017), Jason-3 (2016-present) and Sentinel-6 Michael Freilich (2020-present) satellites. However, calibration and validation (cal/val) is critical if the derived and disseminated geophysical products from altimetry measurements from these and other satellite missions, such as CryoSat-2, SARAL/ALTIKA, HY-2, Sentinel-3 and SWOT (see e.g. [1] for more details), are to provide reliable estimates of the ocean's properties. For example, [2] report how biases in regional sea level rates of ±0.3 mm/year with a strong hemisphere dependence can arise among estimates determined from the T-P, Jason-1 and Jason-2 satellites. This illustrates the importance of undertaking cal/val experiments at multiple sites distributed globally to evaluate the level of geographical consistency among the SSH biases and of the sampling of different oceanographic conditions, with [3] and [4] stressing that such parallel experiments do not constitute duplication.

Cal/val of altimetry satellites has been undertaken using coastline-located tide gauges, e.g. [5], [6]. However, in addition to the tide gauges requiring corrections for vertical land movement, e.g. [7], because tide gauges are not at the altimetry satellite observation point they are an indirect cal/val approach [8] and extrapolation to the altimeter observation points is challenging, requiring accurate models of the ocean tides, dynamic topography and marine geoid, which can be poorly determined in the coastal zone, e.g. [9], [10], [11]. Direct cal/val approaches have been subsequently developed, where the absolute SSH in a global reference frame is determined directly at the altimetry comparison points, thereby overcoming the ocean and geoid model extrapolation problem. Such direct cal/val sites include the Harvest oil platform [12] with a static Global Positioning System (GPS)

receiver located directly under the T-P/Jason track together with a tide gauge, although such platforms are scarce. Static GPS measurements have been made at tide gauges under the T-P/Jason tracks, for example in Corsica [13] and in Tasmania [4]. However, their coastline locations mean they are susceptible to land contamination of both the signals from the altimeter [14] and particularly from the large footprint of the on-board microwave radiometer (MWR) [15], which is used to correct the range measurements for wet tropospheric delay effects. GPS buoys provide a means to overcome land contamination, offset and extrapolation limitations by deploying in-situ directly under the altimeter track to directly measure absolute SSH, e.g. in the Bass Strait [4]. Buoys are also used, such as in Corsica and the Bass Strait, to provide constraints on geoid models and bottom pressure measurements, which subsequently enable absolute SSH measurements and hence altimetry cal/val to be continued outside the times of the actual buoy deployment. However, a buoy requires tens of meters of cabling (hundreds of meters if away from the coastal zone) to be cast together with an anchor to secure it to the sea bed, or tethered to a float or support vessel, making deployment and recovery not straight forward. Buoys provide measurements at single, pointwise locations, although multiple buoys forming an array are now being used for altimetry cal/val (specifically for wide-swath missions such as SWOT) with nine buoys deployed at 5-20 km spacing over ~80 km at the Bass Strait facility (updated from [16]). To obtain logged buoy data, unless they are located within the coastal zone, physical visits are needed because raw data files are typically too large to transfer via satellite communication. Another two altimetry cal/val proposed platforms are reported by [17]. First, the development of a 'towed carpet' GNSS+gimbal based system intended for altimetry SSH cal/val directly in contact with the sea surface and with a vertical antenna. Second, a 'PAMELi' marine drone with GNSS and an acoustic altimeter installed. However, published results to date only include geoid slope measurement [18] and the demonstration of SSH precision of about 2 cm in benign sea states and weather conditions.

Only a small proportion of the global oceans incorporate altimetry cal/val measurements, and each of the cal/val methods used to date has limitations. Recent developments in unmanned surface vehicle technology provide additional potential altimetry cal/val platforms, and in this paper we investigate the use of one such vehicle: the Liquid Robotics Wave Glider equipped with a geodetic Global Navigation Satellite Systems (GNSS) receiver (hereafter termed 'GNSS Wave Glider'). We chose this vehicle because it exhibits almost all the scientific benefits of a GNSS buoy (in-situ, direct, absolute SSH measurement) while also being portable, more versatile and it may be deployed from a small boat in any waters with depth greater than about 10 m. The GNSS Wave Glider also has constant mass, so unlike ships with variable fuel loads, it only experiences small variations in draft, which arise from the wave field and hydrodynamic effects of the water velocity around the platform.

To demonstrate the GNSS Wave Glider multi-satellite altimetry cal/val concept in the absolute sense, we undertook a 13-day experiment in the North Sea in July-August 2016, as described in [19]. The dataset encompassed, by design, scenarios whereby the GNSS Wave Glider was directly located under multiple Jason-2/3 and CryoSat-2 observation tracks. A scheduled positioning under the AltiKa satellite was not possible as the satellite orbit was allowed to drift from its repeating ground track orbit after the boreal spring of 2016. We use the GNSS Wave Glider to undertake cal/val of altimetry SSH measurements in the North Sea from Jason-2 and Jason-3 satellites, on both ascending and descending tracks, as well as CryoSat-2 ascending track measurements, as shown in Fig. 1. When the altimetry satellites were directly above the GNSS Wave Glider the distance from land ranged from 21 to 78 km. We compare the agreements obtained from other cal/val sites globally, which provides an indication of both temporal and geographical consistency and bias, which are essential for the interpretation of altimetry-derived trends in global and regional mean sea level, significant wave height (SWH) estimates, the performance of the MWR and atmospheric corrections, and sea state bias. The results we show to illustrate the GNSS Wave Glider cal/val concept comprise four Jason-2/3 cycles and two CryoSat-2 cycles obtained in a 13-day window. However, it should be noted that to more confidently determine and interpret altimeter-derived biases and trends, larger samples would be needed, encompassing multiple seasons, sea states and meteorological conditions.

We first describe the GNSS Wave Glider instrument and its previous uses. Next we outline the basic cal/val principles of altimetry using GNSS, and then summarize previous SSH, tropospheric delay and SWH cal/val results for Jason-2/3 and CryoSat-2. The data sets used are then described, together with the GNSS and satellite altimetry processing, in particular the error models applied. We then compare SSH estimates at the times of altimetry satellite overpass, and evaluate the quality of the modeled and on-board tropospheric altimetry corrections. Finally, we validate the altimetry estimates of SWH.

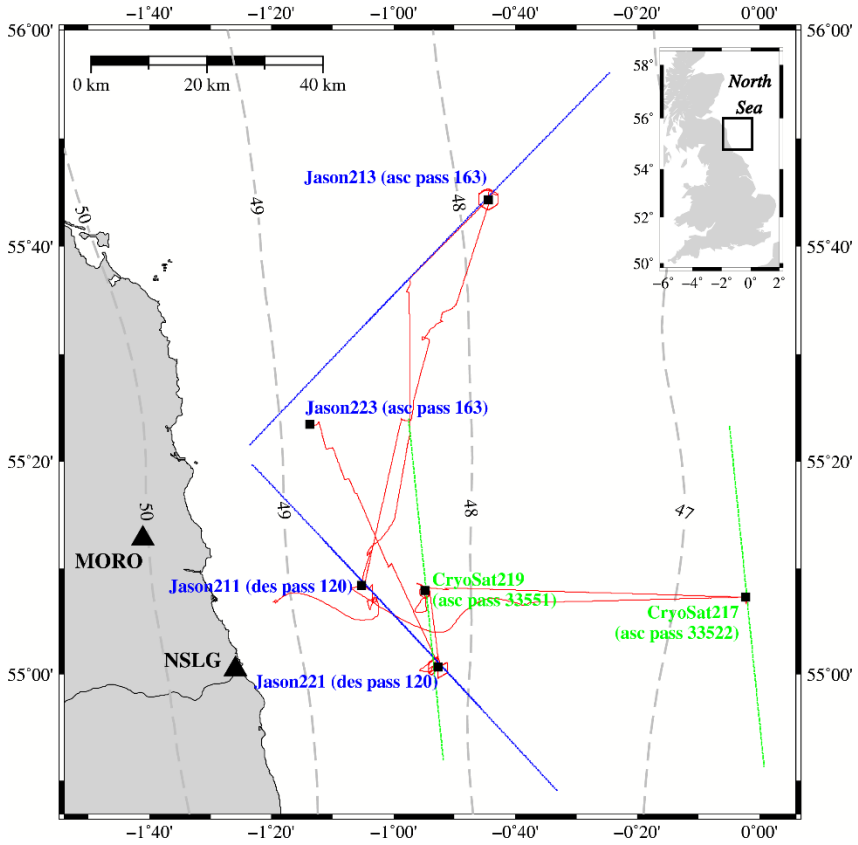

Fig. 1. GNSS Wave Glider (WG) trajectory shown by the red line, location of the WG at times of altimetry satellite passes shown by the black squares, Jason-2/3 altimetry 20 Hz measurement points within 30 km of the WG and at least 9.5 km from land shown in blue, similar CryoSat-2 points shown in green. Onshore GNSS reference stations (MORO and NSLG) are denoted by the black triangles, while the dashed gray lines are 1 m EGM2008 geoid height contours. The three digits after the Jason/CryoSat text denote the day of 2016.

II. The GNSS Wave Glider

The GNSS Wave Glider comprises a ~2 m float attached by a ~7 m long umbilical cord to a rudder and submersible fins which propel the vehicle using wave power alone at a speed over ground of normally 1-2 knots, as described in [20]. A meteorological mast and GNSS antenna are mounted on the float (see Fig. 2) and its on-board instrumentation (including the geodetic GNSS receiver) is housed in payload boxes and powered via solar panels. Navigation to defined waypoints is undertaken by remote web-based piloting via an Iridium communications link, with regular human checks needed, whose frequency ranges from about once per day in areas such as the Southern Ocean to every few minutes in busy shipping lanes such as the Straits of Dover.

Previous works with the GNSS Wave Glider have been undertaken first by [21], who demonstrated 2-5 cm kinematic GNSS precise point positioning (PPP) water surface height measurement precision in the benign conditions of Loch Ness, Scotland. Thereafter, [19] describe the use of kinematic GNSS PPP to continuously measure SSH at 5 Hz in winds gusting up to 20 m/s along the July-August North Sea 490 km deployment track shown in Fig. 1, detecting geoid and dynamic topography gradients with about 5 cm precision, and waves measured with about 20 cm precision. The Wave Glider vehicle is extremely robust, having crossed the Pacific Ocean and Drake Passage unmanned and without a support vessel, and has the benefit over buoys that it may be piloted to any user-defined location globally, and measure additional ocean parameters such as the geoid, dynamic topography, tides and waves between altimetry cal/val locations. The only restrictions are a minimum ocean depth of 10 m, a wave field strong enough to permit adverse surface currents to be overcome, and sufficient sun light to enable solar charging of internal batteries. Typically, about 8 W are needed to power the on-board instrumentation (GNSS receiver, meteorological sensor, onboard navigation system, automatic identification system and, in the future, MEMS inertial navigation sensor (INS)) which can be continuously provided if the mean daily incoming shortwave radiation is greater than ~140 W m^{-2} (based on the vehicle's solar panel area of 0.67 m^2 and a cell efficiency of 10%). At northern hemisphere mid-latitudes, such power can be obtained from about March to September (winter missions may require duty cycling of instruments or a reduced observation sampling regime) and hence continuous operation and data collection of many months is possible. Raw

GNSS data are stored on the on-board computer's hard disk for post-mission retrieval as such files are too large to be transmitted during a mission via satellite communication, but the same limitation applies to many buoy systems (such as the DART or UK WaveNet networks) unless near the coast where 4G telemetry is possible.

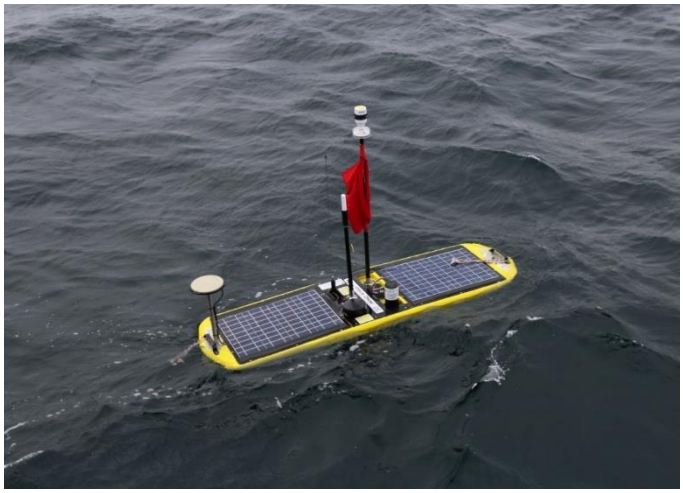

Fig. 2. The GNSS Wave Glider deployed in the North Sea from 28 July to 10 August 2016.

III. Basic Altimetry Cal/Val Concepts

As comprehensively described in, for example, [22], a satellite altimeter to sea surface range measurement ($range_{meas}$) is obtained from the two-way travel time of a radar pulse from the altimetry satellite to the sea surface, which is reflected back to the satellite. The returned radar pulse is fitted by a theoretical waveform function in a process known as retracking. The midpoint along the leading edge provides the time of reflection for range calculation while SWH is inferred from the slope of the leading edge. If the altitude of the satellite (h_{altim_sat}) above a reference ellipsoid in a particular reference frame is known, the altimeter-based SSH (SSH_{altim}) above the same reference ellipsoid may be obtained via:

$$SSH_{altim} = h_{altim\,sat} - (range_{meas} + \Delta range_{propagation} + \Delta range_{geophys}) \quad (1)$$

where $\Delta range_{propagation}$ represents corrections (ionosphere, troposphere and sea state bias) that need to be applied to convert the measured range to a geometric range, and $\Delta range_{geophys}$ denotes geophysical corrections (solid Earth tide and solid Earth component of the pole tide) to be applied before SSH comparison with other sensors (here the GNSS Wave Glider, SSH_{WG}). For the absolute cal/val tests described herein, the resultant bias (SSH_{bias}) is defined as:

$$SSH_{bias} = SSH_{altim} - SSH_{WG} \quad (2)$$

Before computing the SSH bias, noise should be averaged out for both the SSH_{WG} and SSH_{altim} values. For the Wave Glider, random GNSS height measurement imperfections, wave effects and the resulting vehicle dynamic response can be reduced by averaging SSH to a single value over a short time window (here we used 2 min), assuming the horizontal distance traveled is negligible in this window. Before the high-rate (typically 20 Hz) altimetry SSH measurements are averaged to reduce measurement noise (mainly arising from the radar instrument characteristics and inhomogeneities in the several kilometer diameter measurement footprint), the effects of the satellite's motion along its track while recording measurements before and after passing over the Wave Glider's approximate location (here we considered all approach and departure points within 30 km from the Wave Glider but no nearer the coast than 9.5 km) should be taken into account. This is achieved by mapping each SSH_{altim} measurement from the sub-satellite point to the Wave Glider's location by applying relative geoid, ocean tide, dynamic topography, atmospheric and loading displacement corrections. For the tropospheric correction to the measured ranges, a zenith hydrostatic delay (ZHD) is applied which can be accurately determined from numerical weather models such as ECMWF, and also a zenith wet delay (ZWD), which is more difficult to model and observations from an MWR are normally used if the altimetry satellite includes such an instrument.

To compute GNSS Wave Glider SWH estimates, four times the standard deviation of the high-rate (here 5 Hz) GNSS heights over a given time window (here 2 min) may be used, after first applying a high-pass filter to the GNSS ellipsoidal heights or removing from them geophysical modeled values for geoid, dynamic topography, ocean tide, and atmospheric and loading displacement, to leave only the waves. Here the approach of removing modeled values was used.

IV. Jason-2/3 and CryoSat-2 Previous Cal/val Results

There have been substantial efforts by several groups on the absolute cal/val of Jason-2/3 altimetry measurements using GPS at different globally-distributed locations. On using the Jason-2 Geophysical Data Record (GDR) reprocessed 'D' products [23], typical altimetry and GPS-based SSH agreements (biases) have been found to be about −30 to +30 mm. For the Qianli Yan islet in the Yellow Sea, [24] used a combination of GPS onshore reference stations, a GPS buoy and extrapolated geoid and ocean tide models to evaluate biases in the GDR-D Jason-2 products for descending pass 153. Using measurements from 69 cycles during 2013-2014, a bias of +21.0 ± 5.9 mm was obtained, with no discernible trend over the 2 years. For the Gavdos site in the eastern Mediterranean Sea, [25] used onshore GPS reference station data, tide gauge and extrapolated geoid and ocean tide models and found a bias of +3 mm for ascending pass 109 and +6 mm for descending pass 18 for Jason-2 cycles 2-303. Frappart et al. [26] used GPS buoy data gathered in the western Mediterranean Sea about 40 km north-east of Ibiza from September 2013 to obtain a bias of about −20 mm for Jason-2 ascending pass 187 (cycle 191). Bonnefond et al. [13] report a

mean bias of +16 ± 2 mm off Corsica (using onshore GPS and extrapolating for the marine geoid) from 206 Jason-2 passes from 2009 to 2016. The biases from these four studies are considerably reduced from those of ~150-190 mm reported using cal/val with the Jason-2 GDR 'T' products for the 8-month Jason-1 and Jason-2 'tandem' operating phase, such as at the Harvest oil platform in the eastern Pacific Ocean [27], off Corsica [28], in the Bass Strait [29], at Gavdos [30], over Lake Erie in North America [31] and over Lake Issykkul, Kirghizstan [32]. These globally-distributed GDR-T cal/val experiments enabled the identification of errors in the Jason-2 ranges of 180 mm caused by an incorrect antenna reference point, as well as an altimeter pulse repetition frequency truncation error of 25 mm [23]. The Jason-2 GDR-D products thereafter released, as used by [24], [25], [26], [13] and in this study, incorporate corrections for both of these errors.

Jason-3 cal/val experiments have been undertaken for, among others, some of the above-mentioned Jason-2 locations. Crétaux et al. [33] used a boat to obtain GPS measurements of the water surface of Lake Issykkul for Jason-3 cycles 5 and 52 of ascending pass 131, with biases of −28 ± 40 mm obtained when using the *Ocean* retracker and GDR-D products. Using GPS-referenced tide gauges and extrapolated geoid and ocean models, [34] assessed the bias in the Jason-3 SSH from GDR-D products for cycles 77-79 and 101-104 of ascending pass 153 over the Wanshan Islands in the South China Sea, and found a bias of +20.7 ± 49.7 mm. Over Gavdos, [25] demonstrated a Jason-3 SSH bias of −5 mm along the ascending orbit and −7 mm along its descending orbit, based on GDR-D products and the first 80 cycles of Jason-3. During the 8-month Jason-2/3 tandem phase, an SSH bias offset of Jason-3 with respect to Jason-2 of −27 mm was found (Jason-3 SSH lower than Jason-2 SSH), and an offset of +180 mm when ranges were directly evaluated with a ground-based transponder. Yang et al. [35] report a similar Jason-3 minus Jason-2 offset of −29 mm for the Qianli Yan site in the Yellow Sea, and [23] show an offset of −27 mm at Corsica from a Jason-3 minus GPS/geoid bias of −11 ± 4 mm based on 71 passes during 2016-2018. Chupin et al. [36] used a GNSS buoy at Nouméa, South Pacific to enable pressure measurements to be related to the same datum as the tide gauge, whose data were used to compute a 6-year Jason-3 bias of 12 ± 3 mm.

Previous reports of absolute CryoSat-2 SSH cal/val experiments using GPS are limited. Fenoglio-Marc et al. [37] imply SSH versus CryoSat-2 (Synthetic Aperture Radar: SAR mode) mean differences of +83, +20 and −12 mm for three passes in 2012 and 2013 near the Helgoland tide gauge in the German Bight. Bonnefond et al. [38] report on cal/val undertaken in western Corsica using onshore static GPS data co-located at two tide gauges (Ajaccio and Senetosa) 37 km apart, obtaining biases of −746 ± 5 mm using the default options of the ESA Grid-Processing-On-Demand (G-POD) SARvatore service baseline B (https://eo4society.esa.int/resources/sarvatore-g-pod-service-to-users/), but which reduce to −73 mm on applying a known −673 mm range bias. Thereafter, [13] report updated Corsica SAR mode biases of +5 ± 8 mm for Ajaccio and +8 ± 5 mm for Senetosa using passes over 8 years and determined using ESA G-POD baseline C processing.

A key component of accurate absolute SSH determination with satellite altimetry is the correction of the ZWD with MWR observations. Sibthorpe et al. [39] used globally-distributed data and found that ZWDs from the Jason-2 MWR and GPS agreed to within 5 mm and, using a similar approach, [40] found a mean global Jason-2 MWR-GPS 2013-2016 agreement of -5.5 ± 18.4 mm. Zhai et al. [41] computed Jason-3 MWR minus GPS ZWD differences for 3 years around the Wanshan Islands and obtained a difference of -2.3 ± 16.1 mm. Zhu et al. [42] computed a Jason-2 MWR minus GPS mean difference of +3 mm from data for 19 Chinese coastal area sites and similarly a Jason-3 difference of -1 mm, with the uncertainties of these differences in the range 14-21 mm. Vieira et al. [43] computed Jason-2 MWR differences at 60 globally-distributed GNSS stations and obtained RMS differences of about 16 mm when the distance from the coast of the altimetry satellite's nadir pointing was greater than 20 km but less than 50 km. CryoSat-2 meanwhile does not have an MWR, and ECMWF ZWD corrections have been applied by both [38] and [37]. Pearson et al. [44] compared ECWMF zenith total tropospheric delays (ZTDs) with GNSS-estimated ZTDs globally and found a median bias of -3 mm (ECMWF delays greater than GNSS). Also applicable to CryoSat-2 is the GPD+ ECMWF model / MWR / GPS observational ZWD hybrid correction [45].

We were not able to find any publications documenting agreements between Jason-2/3 or CryoSat-2 and GNSS-measured SWH, with such altimetry validations often being undertaken with respect to wave buoys. For Jason-2, [46] compared SWH from the Jason-2 GDR-T product in the Pacific Ocean against wave buoys no more than 150 km from the altimeter tracks, with 23 cm RMS agreements obtained. For Jason-3, [47] obtained a mean RMS SWH difference of 23 cm compared with National Data Buoy Center wave buoys in the Pacific Ocean, Caribbean Sea and west Atlantic Ocean for 5 months of 2019, although the RMS agreements ranged from 12 cm to 40 cm. Passaro et al. [48] found a standard deviation of 15 cm for SWH from the nearest 1 Hz Jason-2 point to a wave buoy in the German Bight. For CryoSat-2 operating in SAR mode, [37] validated SWH against acoustic Doppler current profiler measurements in the German Bight during 2012 and 2013, obtaining a bias of 4 cm and a standard deviation of 14 cm. Abdalla et al. [49] validated CryoSat-2 (SAR mode) SWH estimates against wave buoy measurements from the north east Atlantic Ocean, obtaining a mean difference of 12 cm and a standard deviation of the differences of 36 cm.

V. Data Set and Processing

The GNSS Wave Glider (GNSS WG) shown in Fig. 2 was deployed in the North Sea from 28 July to 10 August 2016,

and was piloted to be directly underneath four Jason-2/3 passes (during the experiment Jason-2 and 3 were deployed in tandem along the same orbit, with Jason-3 lagging Jason-2 in time by 83 s) and two CryoSat-2 passes. The satellite tracks and passes are listed in Table I and shown in Fig. 1, along with the GNSS WG's trajectory taken over the 13 days. For the experiment's duration, SSH was measured with the GNSS WG at a rate of 5 Hz. These SSH measurements were obtained by processing GPS+GLONASS data in PPP mode with the PANDA GNSS software as described in [19], with 5-6 cm agreement obtained between the EGM2008 geoid and the FOAM-AMM7 dynamic ocean topography model, and SWH agreements of 17 cm and 24 cm with the WAVEWATCH III model and the Cefas Tyne-Tees WaveNet buoy, respectively. The GNSS-estimated heights of the antenna reference point were in the IGb08 reference frame (center of mass of the solid Earth, atmosphere and oceans: CM) above the GRS80 ellipsoid, with corrections for the solid Earth component of the pole tide and solid Earth tide applied according to the IERS2010 Conventions [50], yielding coordinates in a conventional tide-free system. No loading displacement corrections were applied, whilst ZTDs were estimated every hour, via residual corrections to the GPT-2 model and applying the GMF mapping function [51] with a 7-degree elevation angle cut-off. ZWDs were then obtained by subtracting from the ZTD the ZHD computed according to the ECMWF numerical weather model. The length of the pole on which the GNSS antenna was mounted (see Fig. 2) was 0.34 m, and this 0.34 m offset was applied to map the GNSS-estimated ellipsoidal heights from the antenna reference point to the surface of the WG's float, which was assumed to represent the measured water level and hence the reference for SSH_{WG}. This was deemed appropriate because, as can be seen in Fig. 2, the aft of the vehicle's float on which the antenna was mounted, sits lower than the center of the float's upper surface (which is 1-2 cm above the water surface). We do however acknowledge that further, comprehensive experiments are needed, such as in a laboratory or co-located with a tide gauge, to more accurately determine the offset, with such experiments compounded by the challenge that the tilt of the WG in response to waves and different sea states must also be accounted for. We also recognize that the applied phase center variation and wind up corrections should account for the GNSS antenna's variable orientation, which was not attempted here but has been by, for example, [52]. Such orientation measurements can be obtained by incorporating an INS as has been undertaken by [53]. The inclusion of antenna tilt corrections will take on increasing importance if the antenna height is increased from that used here to overcome spray in rougher sea states. Note that the 0.34 m antenna height stated and applied here is different from the 0.35 m stated antenna height in [19] for the same North Sea data set. This 0.35 m statement in [19] was a mistake, and it should have been stated as 0.34 m. For the Loch Ness study of [21] using the same Wave Glider, a different antenna pole from that used in this North Sea data set was used, which had a length of 0.36 m. Furthermore, [52] have shown that the antenna tilt and height on a GNSS buoy can be impacted by water velocity with respect to the platform (induced by either water current or tether tension changes), and similar antenna tilt and height corrections will also likely apply to the GNSS Wave Glider (depending on its hydrodynamic properties) as it holds station at an altimetry cal/val point.

We used the kinematic PPP mode of GNSS processing rather than post-processed kinematic (PPK) since the distance of the WG from the nearest distance onshore reference station is predominantly greater than the maximum baseline length of 20-30 km recommended by [8] for 1-2 cm filtered accuracy positioning. PPP has been used on multiple previous occasions for Jason-2/3, Sentinel-3A and SARAL altimetry cal/val. These include off Ibiza by [26] for Jason-2 and SARAL using GPS buoys; over Lake Issykkul on a boat, measuring the water surface height with 2 cm precision [33]; at Noumea, South Pacific [36] using a GNSS buoy combined with a bottom pressure sensor and tide gauge for Jason/Sentinel-3A crossover point cal/val. Haines et al [54] used kinematic PPP GPS to obtain SSH measurements for a buoy in the Pacific Ocean on Daisy Bank continuously over 120 days of 2016, in waves ranging from 0.7-3.8 m (mean SWH 1.7 m). PPP GPS SSH values agreed with those from 23 passes of Jason-2/3 with 32/34 mm standard deviation and -4±7 mm / -43±7 mm bias, respectively. The PPP GPS ZWD estimates agreed with those from the Jason MWRs to mm level bias and 7-8 mm scatter, GPS-measurements of SWH agreed to about 10 cm bias and 10 cm scatter with all of a wave buoy, Jason-2 and Jason-3 (23 passes). Other successful kinematic PPP GNSS SSH measurement includes the use by [17] of kinematic PPP GPS+GLONASS+Galileo to obtain SSH values off New Caledonia for a towed carpet and GNSS buoy 45-400 m apart and, after correcting for the geoid, obtained SSH agreements between the two instruments of better than 25 mm standard deviation. Kato et al. [55] undertook kinematic PPP analysis of GEONET data and obtained better than 26 mm height standard deviation over 10 days, then applied this to a buoy offshore. Liang et al. [56] undertook 60 days of kinematic PPP observations at a GNSS buoy 70 km off the China coast in the Yellow Sea, and obtained 1 cm amplitude agreements for M2, S2, O1 and K1 tidal harmonics compared with pressure sensors. Fan et al. [57] showed better than 20 mm RMS agreements across all three components between kinematic PPP and PPK (for a short 2 km baseline) on a sailing vessel, and then better than 40 mm for a holding mode. On the GNSS WG, [21] obtained a standard deviation of 23 mm for PPP-PPK water surface height differences on Loch Ness over 25 hours and for up to 25 km PPK baselines, with a mean difference of 5 mm.

Both PPP and PPK GNSS processing modes have their limitations, with both being affected by outages in signal tracking caused by spray effects over the GNSS antenna, e.g. [19]. Watson et al. [4] considered reliable PPK-based SSH values for a GNSS buoy to be obtained in maximum Beaufort scale sea states of 3 to 4, although overcome this somewhat in [29] by increasing the antenna height. Zhou et al. [53] report problems with PPP processing failures on one of four 3-6 day

GNSS/INS buoy deployments in the Bass Strait that did not arise for PPK, attributing this to receiver clock drift. However, we note that this is speculation and no results or evidence are presented. The RMS SSH differences of (GNSS buoy-mooring) obtained by [53] after removal of outliers were 1.7, 2.6 and 1.5 cm for PPP, and 1.7, 2.6 and 1.9 cm for PPK, with a slightly higher percentage of outliers removed for PPP on 2/3 deployments than PPK, but PPP had fewer outliers than PPK on their third deployment. The SSH spectra identify periods where the PPK solution is noisier than the PPP, and vice versa. Neither PPP nor PPK approaches have necessarily retained 100% of the processed GNSS data points in order to obtain the required SSH-based parameters. For example, for PPK in the Bass Strait, [53] employed first a 3-sigma and then a 1.5 interquartile range approach to obtain clean SSH solutions, while De Marez et al [58] for PPP processing in the Pacific Ocean only used GPS-based SSH values for SWH less than 4 m to constrain a model of the wavenumber-frequency content of balanced SSH variance. Note however, that in the analysis presented herein, we have used all PPP-based 5 Hz GNSS SSH values during the identified windows without the need for any removal of outliers. We also point out that critical for PPP is the accurate estimation of tropospheric delay ([59] cite this as their limitation), with [60] showing that an appropriate tropospheric process noise is crucial for accurate ZWD and hence PPP-based height estimation. We will show in Section VI(B) that we estimated the ZWD on board the WG to 2-3 mm bias and 9 mm standard deviation, thus the impact on heights is no more than 3.5 cm, following the 3-4 zenith tropospheric delay error mapping to epoch-by-epoch height estimation shown by [61], following on from the similar "rule-of-thumb" of [62]. Integer ambiguity resolution is possible (but not standard) in kinematic GPS PPP processing, although [63] showed how kinematic GPS+GLONASS float PPP (as used here) has the same precision as integer-fixed GPS PPP.

Further GNSS WG PPP height estimation quality tests to those of [19] were undertaken. As mentioned in [19], continuous GNSS data at 1 Hz from the Ordnance Survey onshore reference station MORO (see Fig. 1) were obtained and processed using the same PANDA GPS+GLONASS PPP approach as the WG, with a height standard deviation (precision) of 20.3 mm obtained over the 13-day experiment. Thereafter, to assess the accuracy of the GNSS WG kinematic PANDA PPP coordinates, they were compared with relative post-processed kinematic (PPK) coordinates, as is widely used to assess PPP coordinate accuracy, e.g. [64], [65], [66]. However, as recommended by [8], PPK for SSH determination should preferably be limited to no more than 20-30 km baseline lengths, so here PPP-PPK comparisons are only considered for such instances. Only on DOY 210 and for the first seven hours of the WG mission was the distance from the MORO reference station less than 30 km and hence this criterion fulfilled. The Leica Infinity v4.0.2 software was used to obtain a 1 Hz GPS+GLONASS PPK solution for the GNSS WG with respect to the mean PANDA PPP-based computed reference coordinates for MORO and the PPP-PPK SSH differences are plotted in Figure S1. All 1 Hz PPK epochs in this window were integer-fixed, and using all data points (no outlier removal of PPP or PPK points) the mean PPP-PPK SSH differences were 7.8 mm and their standard deviation was 18 mm. These PPP-PPK height differences are similar to those obtained by [21].

The altimetry products we used to compute SSH, SWH and ZWD were the GDRs obtained from AVISO for Jason-2 ('D' products) and Jason-3 ('F' products), and the CryoSat-2 SAR Geophysical Ocean Product (GOPR) baseline C [67] obtained from ESA. For SSH comparisons with the GNSS WG, we used the 20 Hz products, and to enable averaging of altimetry measurement noise, extracted all range data points within ±30 km of the GNSS WG at the time of overpass (over this 60 km distance the SSH values remained approximately linear as shown in Fig. 3). Except for the Jason-2/3 comparison on DOY 223, the point of closest approach from the GNSS WG for each pass was less than 1 km (Table I). To reduce measurement degradations from signal land contamination, we removed any data points within 9.5 km of land, according to the Generic Mapping Tools version 4.5.6 full resolution coastline [68]. This 9.5 km cut-off is approximately equal to the radius of the Jason-2/3 footprint, and compatible with the reporting of [69] that the proportion of Jason valid measurements decreases considerably when closer than about 10 km from the coast. This 9.5 km filter only affected the Jason-2/3 values used on DOY 211 and DOY 223: data points on DOY 223 less than 9.5 km from land exhibited SSH values many meters greater than those further offshore. All CryoSat-2 points were at least 27 km from land. These defined limits led to 198-205 20 Hz data points for use from Jason-2/3 and CryoSat-2 on all days considered except for DOY 223, when there were 135 Jason-2/3 data points.

At each 20 Hz epoch the Jason-2/3 and CryoSat-2 range measurements were corrected for ZHD and ZWD, solid Earth tides, solid Earth component of the pole tide and ionospheric delays using the corrections listed in Table II. For both Jason-2/3 and CryoSat-2, ZHDs were applied using the ECMWF model. ZWDs for Jason-2/3 were applied using measurements from the on-board MWR, which records brightness temperature on three channels, and to reduce land contamination effects the mixed pixel algorithm of [70] was used. Because CryoSat-2 does not have an MWR instrument on-board, the GPD+ model [45] was used to correct for the wet delay. The GDR/GOPR-provided ECMWF/MWR/GPD+ tropospheric delays were interpolated from 1 Hz to 20 Hz (tropospheric delay does not vary over timescales of a few seconds, so this interpolation causes no loss of accuracy), while permanent tide [50] and T-P to GRS80 (Jason-2) and WGS84 to GRS80 (Jason-3 and CryoSat-2) ellipsoid corrections were also applied to ensure compatibility with the GNSS SSH ellipsoidal heights. Hence both the GNSS and altimetry heights were expressed as 'tide free', and not the altimetry default of 'mean tide'. The Jason GDRs contain parameters derived relative to several retrackers. Over the

oceans the Maximum Likelihood Estimation (MLE) retrackers with three or four parameters are available. In addition, Jason-3 has results for an adaptive retracker. As recommended in the handbook [71], MLE4 (four parameters) was adopted for both Jason satellites, with the MLE4 ku band range and ionospheric correction. For CryoSat-2, the SAR Altimetry Mode Studies and Applications (SAMOSA) retracker v2.3 [72] was used. Sea state bias corrections were applied, using MLE4 for Jason-2/3 and for CryoSat-2 those based on empirical fits to CryoSat-2 GOP baseline B data. The corrected ranges were then subtracted from the satellite altitude to obtain SSH_{altim} per 20 Hz epoch. For each epoch, the SSH_{altim} value was mapped from the sub-satellite point to the GNSS WG location by applying relative marine geoid (using EGM2008: [73], [74]) and relative ocean tide (using EOT20, including loading: [75]) corrections, and then averaged. Relative dynamic atmospheric corrections were applied for Jason-2, Jason-3 and CryoSat-2 using the barotropic MOG2D model [76]. These relative atmospheric corrections had a 0-1 mm effect on the SSH bias except for Jason-2/3 on DOY 223 when the effect was 5-6 mm.

For SWH, values for Jason-2/3 (within 30 km of the GNSS WG and no nearer land than 9.5 km) were obtained from the 1 Hz GDR products and then averaged. The 1 Hz values, obtained via the MLE4 approach [77], were used rather than the 20 Hz SWH values as the latter are susceptible to discretization problems from the bin size/gate number of the altimetric waveform. For CryoSat-2, 1 Hz SWH values were obtained from the GOPR products with SAMOSA v2.3 retracking. The GNSS WG SWH was computed as four times the standard deviation of the 5 Hz GNSS wave heights computed in [19], using a 2-min window.

In the altimetry versus GNSS WG comparison results included hereafter, only one set of GNSS WG-based SSH, ZWD and SWH is used for each of the six cal/val locations. While the Jason-2 and Jason-3 measurements are offset in time by 83 s and their orbital ground tracks differ by a few hundred meters, the maximum north-south and east-west movement of the WG during the 83 s interval between any of the four considered Jason passes over the WG was only 37 m. Therefore the same GNSS WG estimated SSH, SWH and ZWD values are used for both Jason-2 and Jason-3 cal/val in the following sections, centered in time about the mean of the two epochs of the Jason-2 and Jason-3 respective points of closest approach to the WG. 2 min of 5 Hz GNSS height estimates were averaged per satellite pass to obtain the values for SSH_{WG} used in the comparisons, and similarly 2 min of GNSS WG SWHs were used for comparing with the altimetry values. For the GNSS versus altimetry SSH and SWH comparisons that we later show, we computed the comparisons with GNSS window averaging bin lengths ranging from 1 min to 15 min and found that the range in values were within the system noise (Figure S2 and Table S1). Hence we chose a 2 min window, over which WG horizontal motion and ocean tide effects are negligible: beyond 15 min, ocean tide effects (which we did not apply for our absolute SSH comparisons, only for altimetric relative corrections for mapping from nadir to WG location) started to become significant. We note though that our optimal averaging window has only been computed using a small number of altimetry passes, with [53] suggesting an optimal window length of 25 min, but which was based on an analysis of GNSS buoy against mooring SSH values, in which ocean tide effects were differenced away..

TABLE I

ALTIMETRY SATELLITE META DATA FOR ABSOLUTE CAL/VAL COMPARISONS WITH THE GNSS WAVE GLIDER (WG). TIMES AND LOCATIONS FOR JASON-2/3 ARE GIVEN FOR THE MID-POINT BETWEEN THE JASON-2 AND JASON-3 POINTS OF CLOSEST APPROACH (POCA), WITH JASON-3 LAGGING JASON-2 IN TIME BY 83 S.

Satellite	**Pass (asc/des), cycle**	**Time (UTC) and Day of 2016**	**WG WGS84 latitude, longitude**	**Distance of POCA from WG (JA2, JA3)**
Jason-2/3	Pass 120 (des), cycle 297 (JA2) and 17 (JA3)	17:42, 211	55° 08′ 22″, −01° 05′ 16″	0.7 km, 0.4 km
Jason-2/3	Pass 163 (asc), cycle 297 (JA2) and 17 (JA3)	10:40, 213	55° 44′ 23″, −00° 44′ 28″	0.3 km, 0.6 km
CryoSat-2	Pass 33522 (asc)	11:18, 217	55° 07′ 17″, −00° 02′ 18″	0.3 km
CryoSat-2	Pass 33551 (asc)	11:16, 219	55° 07′ 54″, −00° 54′ 51″	0.2 km
Jason-2/3	Pass 120 (des), cycle 298 (JA2) and 18 (JA3)	15:41, 221	55° 00′ 41″, −00° 52′ 40″	0.6 km, 0.3 km
Jason-2/3	Pass 163 (asc), cycle 298 (JA2) and 18 (JA3)	08:38, 223	55° 23′ 30″, −01° 13′ 42″	5.0 km, 5.4 km

TABLE II

JASON-2/3 GEOPHYSICAL DATA RECORDS (GDRS) AND CRYOSAT-2 GEOPHYSICAL OCEAN PRODUCTS (GOPRS), TOGETHER WITH CORRECTIONS APPLIED FOR SATELLITE ALTIMETRY SSH CALCULATION. THE CORRECTIONS DENOTED BY AN ASTERISK HAVE BEEN COMPUTED EXTERNALLY FROM THE GDRS / GOPRS: ALL OTHER CORRECTIONS LISTED AND APPLIED WERE OBTAINED FROM THE GDRS / GOPRS. RELATIVE CORRECTIONS DENOTE THOSE APPLIED ONLY IN A RELATIVE SENSE PURELY TO MAP THE RANGE MEASUREMENTS FROM THE ALTIMETER NADIR LOCATION TO GNSS WG LOCATION.

Parameter / error source		**Altimetry satellite**		
		Jason-2	**Jason-3**	**CryoSat-2**
Altimetry product		GDR-D	GDR-F	GOPR baseline C
Orbit		DORIS+GPS	DORIS+GPS	DORIS
Reference frame		ITRF2008	ITRF2014	ITRF2008
Reference ellipsoid		TOPEX++	WGS84	WGS84
Retracker		MLE4	MLE4	SAMOSA v2.3
Propagation corrections	Hydrostatic troposphere	ECMWF	ECMWF	ECMWF
	Wet troposphere	Radiometer	Radiometer	GPD+
	Ionosphere	MLE4 Ku and C band dual frequency combination	MLE4 Ku and C band dual frequency combination	Global Ionospheric Map (GIM)
	Sea state bias	MLE4	MLE4	Empirical fits to CryoSat-2 GOP baseline B data
Geophysical corrections	Solid Earth tide	IERS 2010 Conventions (expressed as tide free)*	IERS 2010 Conventions (expressed as tide free)*	Cartwright and Edden (expressed as tide free)* [78]
	Solid Earth pole tide (excluding ocean)	IERS 2010 Conventions*	IERS 2010 Conventions*	IERS 2010 Conventions*
	Geoid	EGM2008 relative corrections only*	EGM2008 relative corrections only*	EGM2008 relative corrections only*
	Ocean tide, including loading	EOT20 relative corrections only*	EOT20 relative corrections only*	EOT20 relative corrections only*
	Atmospheric forcing	High frequency MOG2D relative corrections only	MOG2D dynamic atmospheric relative corrections only	MOG2D dynamic atmospheric relative corrections only

++converted to GRS80

VI. Altimetry Cal/Val Results

A. Sea Surface Height Biases

The SSH biases between the 20 Hz averaged altimetry and GNSS WG SSH values per pass for each of Jason-2, Jason-3 and CryoSat-2 are listed in Table III. It can be seen that for all four Jason-2 and Jason-3 passes, the biases are within −40 to +1 mm, which are almost commensurate with the cal/val results of the previous studies mentioned in Section III, although none considered the North Sea. On average, Jason-2 SSH is slightly greater (higher) than Jason-3 by 7 mm, with mean 20 Hz SSH biases of −16 mm and −23 mm, respectively. This +7 mm average Jason-2 minus Jason-3 SSH offset is less than the +30 mm offsets reported over Gavdos by [25], over Corsica by [13] and over the Yellow Sea by [35], although only four values contribute to our Jason-2 and Jason-3 averages, so the difference should be interpreted with caution. We also note that further caution is needed when comparing Jason-2 GDR-D and Jason-3 GDR-F product values as undertaken here because the two products do not use the same reference frame. The Jason-3 GDR-F products which we used are in ITRF2014 whereas the Jason-2 products are in ITRF2008. A principal difference between ITRF2014 and ITRF2008 is that the effects of time series offsets and seasonal variations, not just linear trends, were incorporated in the determination of epochal positions for ground stations [79] whose data and coordinates are used in the satellite orbit determination. Hence such changes may affect the resulting altimetry SSHs, although the exact impact and value of any resulting reference frame induced altimetry bias change requires an in-depth additional study.

Also included in Table III are the Jason-2 and Jason-3 SSH biases obtained when using the 1 Hz SSH data points, although the values (and the Jason-2 and Jason-3 differences) are not identical to the 20 Hz averages, with a 16 mm difference arising for Jason-3 on DOY 223. This is because, obviously, there are fewer 1 Hz points than 20 Hz points, which can be seen from Fig. 3, that shows plots of the raw 20 Hz and 1 Hz SSH values within ±30 km of the GNSS WG for sample passes of (a) Jason-2 (DOY 221), (b) Jason-3 (also DOY 221) and (c) Jason-3 on DOY 223 when the satellite was further from the GNSS WG and the implementation of the 9.5 km distance to land cut-off was significant. The noise of the individual SSH measurements can be seen from Fig. 3, as well as how the individual 20 Hz and 1 Hz SSH values are corrected for first relative geoid and then relative ocean tide effects, showing that both geoidal and tidal effects within ±30 km of the WG are approximately linear. Furthermore, before the average geoid, tide and atmospheric-corrected altimetry SSH is computed in order to compare with the GNSS WG SSH, the lack of slope in the bottom panes of Figs. 3a, b, c and d show that any linear trends have been successfully removed by the application of the relative geoid, ocean tide and atmospheric corrections. Note that the absence of data points within 5 km of the GNSS WG in Fig. 3c is because the GNSS WG was not directly situated underneath the Jason-2/3 overpassing track on DOY 223, but 5 km away. Similar plots for the Jason-2/3 DOY 211 and 213 passes, and Jason-2 DOY 223 pass are provided in the Supplementary Material (Figs. S3-S10).

The CryoSat-2 SSH biases are also listed in Table III and, for DOY 217, equivalent sample plots of SSH as raw, geoid-corrected and geoid plus tide (and atmospheric) corrected values provided in Fig 3d (the equivalent plot for DOY 219 is provided in the Supplementary Material, Fig. S12). As for Jason-2/3, it can be seen that the geoid and ocean tide effects on the SSH values are approximately linear within ±30 km of the WG, and the resultant SSH biases are −29 mm on DOY 217 and +18 mm on DOY 219 when using the 20 Hz values, and −31 mm and +20 mm when using the 1 Hz SSH values. These are at least commensurate with the −12 to +83 mm biases obtained for the German Bight by [37], although the −29 mm and +18 mm biases are larger than the +5 mm and +8 mm biases obtained around Corsica by [13].

While the Jason-2/3 and CryoSat-2 SSH biases of a few centimeters found for the North Sea are almost commensurate with those obtained elsewhere in the aforementioned studies, and demonstrate the suitability of the GNSS WG for altimetry SSH cal/val, it should be noted that one limiting factor is the accuracy with which the GNSS antenna to water surface offset is known. We estimate this as having an error of about 1 cm, because (as stated in Section V) the base of the pole supporting the GNSS antenna on the WG is deemed to be level with the average water surface. However, a further experiment is needed to confirm this, which is not straight forward as the dynamic response of the WG to both the waves themselves and propulsion via its umbilical cord must be taken into account, ideally including roll and tilt.

Another factor contributing to the quality of the results and size of the SSH biases is the sea state / meteorological conditions. We showed in [19] that GNSS tracking outages started to arise (most likely from spray and breaking waves over the 0.34 m high antenna) when the wind gusted above 15 m/s, which degraded the proportion of reliable position estimates available, although these did not depend directly on SWH (2-3 m swell with mean winds of up to 10 m/s led to no tracking outages, for example). None of the six cal/val windows considered here coincided with wind speed gusts of greater than 15 m/s, with mean wind speed varying from 5-10 m/s (see Table S2) and no tracking outages occurred [19]. We computed the standard deviation (scatter) of the SSH residuals, and found for the 20 Hz data that these were 64-82 mm for Jason-2, 62-82 mm for Jason-3 and 41-42 mm for CryoSat-2. These standard deviations are listed in Table S2, with this limited sample not showing any direct dependence of SSH standard deviation on SWH. While the altimetry sea state bias (SSB) increases with SWH, up to SWH of about 2.5 m, an RMS error of about 2 cm is expected according to [80]. This is commensurate with the SSH biases of up to about 3 cm that we obtain here, although we did not experience larger SWH conditions to be able to assess the impact of all sea state ranges on the GNSS Wave Glider's cal/val capability. While,

having averaged the GNSS-derived heights, we did not see any increase in SSH bias with increasing SWH, potential effects of surface waves and currents should be investigated in the future, such as the use of an INS to account for these and overcome any such potential SSH biases with SWH.

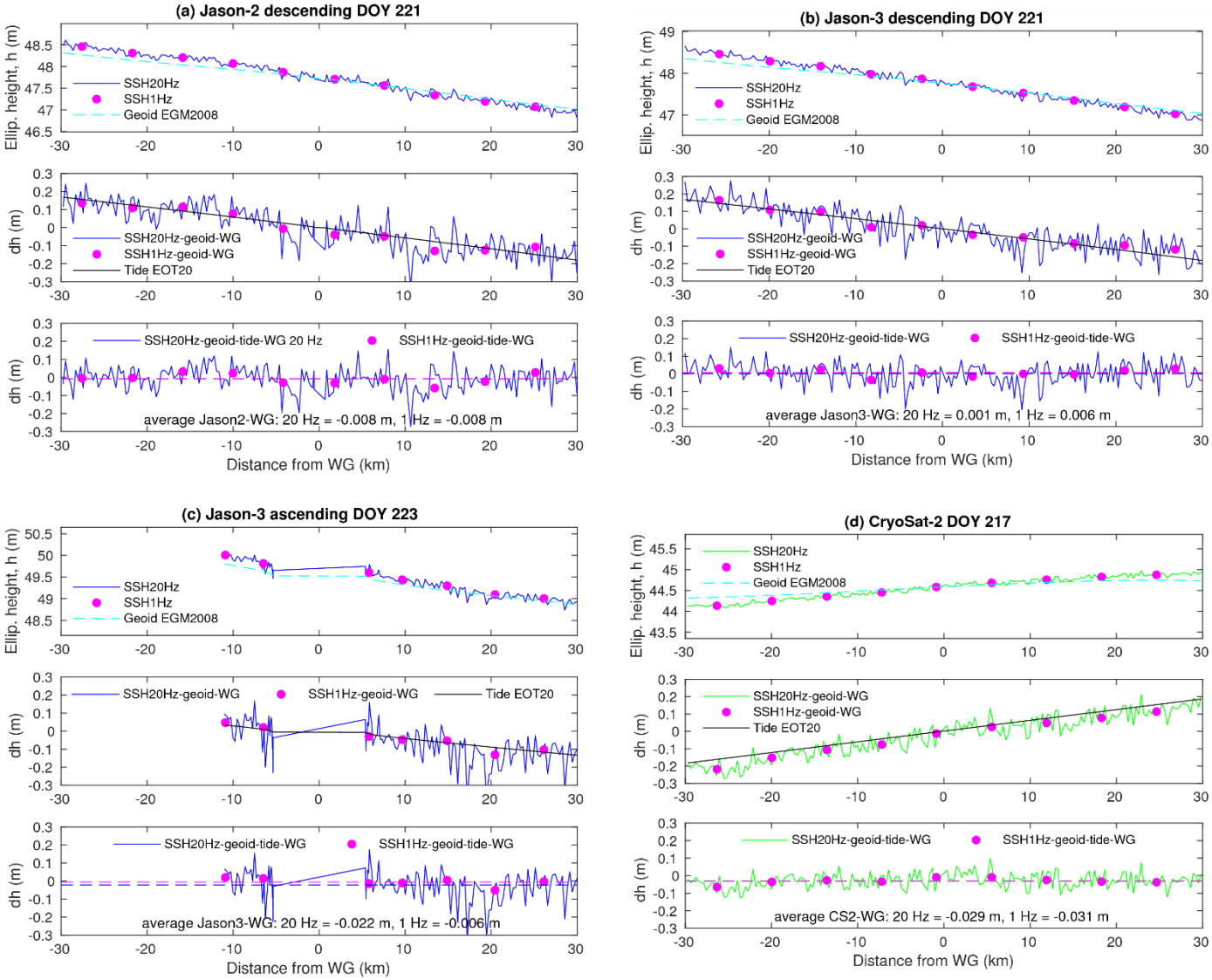

Fig. 3. Sea surface height (SSH) from altimetry and their differences with respect to the GNSS Wave Glider (WG) for sample passes of Jason-2/3 and CryoSat-2: (a) Jason-2 on DOY 221, (b) Jason-3 also on DOY 221, (c) Jason-3 on DOY 223 and (d) CryoSat-2 on DOY 217. For each of (a), (b), (c) and (d), the top pane shows the altimetry 20 Hz ellipsoidal SSH, together with the GDR/GOPR 1 Hz values, and superimposed are the EGM2008 geoid heights relative to those at the GNSS WG, added to the median altimetry-measured SSH. The middle pane shows the geoid-corrected 20 Hz SSH and the ocean tide relative to that at the GNSS WG. The bottom pane shows the difference between the 20 Hz altimetry SSH values (corrected for relative geoid, ocean tides and atmospheric forcing) and the GNSS WG SSH, and the average difference. DOY = day of year. Satellite approach distances from the WG are denoted as negative, departure distances as positive.

TABLE III

BIASES (DIFFERENCES) BETWEEN SEA SURFACE HEIGHT (SSH) AND ZENITH WET TROPOSPHERIC DELAY (ZWD) OBSERVED BY THE ALTIMETRY SATELLITES AND THE GNSS WAVE GLIDER (WG). ALTIMETRY SSH VALUES USED ARE AVERAGES OF ALL POINTS WITHIN 30 KM OF THE WG BUT NO CLOSER THAN 9.5 KM FROM LAND, MAPPED TO THE GNSS WG'S LOCATION, SHOWN FOR BOTH 20 HZ AND 1 HZ RECORDS (1 HZ VALUES IN PARENTHESES). ZWDS FOR JASON-2/3 (1 HZ VALUES ONLY USED) ARE FROM THE MICROWAVE RADIOMETER (MWR) AND THE ECMWF MODEL FOR THE ALTIMETRY POINT NEAREST THE WG. FOR CRYOSAT-2, THE ZWD MODEL IS GPD+. ALL VALUES ARE IN MILLIMETERS AND REPRESENT ALTIMETRY MINUS WG.

Day of 2016	**SSH 20 Hz (1 Hz) – GNSS WG**			**ZWD MWR (1 Hz) – GNSS WG**		**ZWD Model (1 Hz) – GNSS WG**	
	Jason-2	**Jason-3**	**CryoSat-2**	**Jason-2**	**Jason-3**	**Jason-2/3**	**CryoSat-2**
211	−14 (−14)	−40 (−40)		−16	−14	+7	
213	−30 (−31)	−32 (−21)		−10	−6	0	
217			−29 (−31)				−3
219			+18 (+20)				+5
221	−8 (−8)	+1 (+6)		−14	−8	+7	
223	−10 (−7)	−22 (−6)		−20	−12	−5	
Mean	−16 (−15)	−23 (−15)	−6 (−6)	−15	−10	+2	+1

B. Zenith Wet Tropospheric Delay Validation

A key contributor to the attainable accuracy of SSH from satellite altimetry is the tropospheric delay correction applied, and because independent ZWD estimates were obtained from the GNSS WG's data processing, here we assess the accuracy of the GDR/GOP product ZWDs applied to the altimetry measurements and hence their contribution to the SSH_{bias} values.

Before assessing the accuracy of the altimetry product tropospheric delays, the GNSS WG kinematic PPP-estimated tropospheric delays were themselves quality-assessed by comparing with ZWDs obtained for the onshore, static NSLG GNSS reference station (see Fig. 1) from the Nevada Geodetic Laboratory (NGL) [81], computed every 5 min using the Gipsy-X v1.0 software with the ECMWF-based ZHD values [82] subtracted from the Gipsy-X estimated ZTDs to leave the ZWD. The time series of ZWD estimates over the 13-day experiment for both the GNSS WG kinematic and the NGL static GPS processing (the 5 min Gipsy-X outputs were averaged to hourly values to match those of the GNSS WG) are shown in Fig. 4. The hourly differences between the GNSS WG and NSLG ZWDs are also shown in Fig. 4 and, while the distance from the GNSS WG to NSLG (situated 7 m above Ordnance Datum Newlyn) varied from 14 to 94 km over the 13-day experiment, the mean of the hourly GNSS WG minus NSLG ZWD differences is only +2.6 mm, and the standard deviation of the differences is 9.1 mm. These agreements suggest that the GNSS WG kinematically-estimated ZWDs are sufficiently accurate to be used to quality control the altimetry product tropospheric delays, and at least commensurate with the estimated accuracy of the MWR ZWD mixed-pixel algorithm, which was suggested by [70] to be better than 8 mm when 15 km from land and 12 mm when 5 km from land. We note however that this suggested accuracy is obtained from only testing in one season, and when the GNSS WG experienced fairly benign sea states and meteorological conditions. The same caveat applies to all the comparisons in this section.

In addition to the ZWD, a potential error contributor to the tropospheric delay corrections applied to the altimetry measurements is the ECMWF-based ZHD, and any errors in these will map directly into the Jason-2/3 and CryoSat-2 SSH values. To provide an indication of the precision and accuracy of the ECMWF-based ZHDs from the GDRs/GOP applied to the altimetry range measurements, modeled ZHDs were computed at the 6-hourly ECWMF model temporal resolution according to [82] for the NSLG onshore GNSS reference station. This station has a Paroscientific Met4 sensor co-located which logs pressure measurements every 5 min, and which were then used to compute ZHDs according to [83]. The NSLG Met4 and ECMWF ZHD time series are shown in Fig. 5 (upper pane), with the differences at the 6-hourly common epochs also shown in Fig. 5 (lower pane). Over the 13-day experiment, the mean difference was 0.7 mm and the standard deviation of the differences was 1.2 mm, suggesting that any impact of ECMWF-based ZHD correction errors on the Jason-2/3 and CryoSat-2 SSH values is only about 1 mm. ECMWF-based modeled ZHDs also had an impact on the quality of the GNSS-estimated ZWDs that were used to quality control the altimetry MWR and modeled ZWDs, because the modeled ZHD was removed from the ZTD that is directly obtained from the GNSS Wave Glider's PPP processing. Hence in Fig. 5 we also show the modeled ECMWF ZHD for the Wave Glider and the difference with respect to NSLG. The mean and standard deviation of these differences are only 1.3 mm and 1.8 mm respectively, despite the Wave Glider being up to 90 km distant from NSLG. Hence any errors in the GNSS WG estimated ZWDs due to ZHD model errors are also only about 1 mm.

For each Jason overpass, the MWR-measured ZWD was extracted for the single measurement epoch nearest the GNSS WG (the variation of MWR ZWD with distance from the GNSS WG was smooth, so the nearest point was taken to be the most representative of atmospheric conditions at the GNSS WG). These MWR-based ZWDs, as well as modeled ZWDs (ECMWF for Jason-2/3, GPD+ for CryoSat-2) from the nearest measurement point are shown in Fig. 4 (upper pane).

Their differences (altimetry satellite ZWD minus GNSS WG estimated ZWD) are listed in Table III. For all four Jason-2/3 overpasses, the differences between the MWR-based ZWD and the GNSS ZWD have a similar measurement accuracy for both Jason-2 and Jason-3, ranging from −20 mm to −6 mm. The MWR-based ZWDs are always shorter than the GNSS WG ZWDs, with mean differences of −15 mm for Jason-2 and −10 mm for Jason-3. The 6-20 mm errors obtained for the Jason-2/3 MWR-based ZWDs applied to the altimetry ranges are commensurate with the ~16-20 mm ZWD RMS errors found for the Jason-2/3 MWRs by [43] and [84], when comparing respectively with onshore static GPS ZWDs and radiosonde wet delays globally, as well as the mean global MWR versus GPS ZWD comparisons reported by [40] of -5.5 ± 18.4 mm. The distance from land of the Jason-2/3 sub-satellite point nearest the GNSS WG used for the ZWD comparisons ranged from 21 km on DOY 223 to 55 km on DOY 213, with a similar ZWD accuracy with respect to the GNSS WG for all four overpasses. This apparent lack of land contamination is in sympathy with the findings of [43] that land contamination effects arise when closer than 20-25 km from the coast, but it should be noted that [42] suggest that MWR contamination effects can arise even when 40-50 km from the coast.

For CryoSat-2, the differences between the GPD+ modeled ZWD and GNSS WG estimated ZWD are −3 and +5 mm for DOY 217 and 219, respectively. Meanwhile, the ECMWF modeled ZWDs for Jason-2/3 are actually closer to the GNSS WG ZWDs than the MWR-based ZWDs, with (model minus GNSS WG) differences ranging from +7 mm to −5 mm and a mean difference of +2 mm (the Jason-2 and Jason-3 differences are less than 1 mm and not shown separately in Table III because the two points of closest approach are only a few kilometers apart).

We recomputed the Jason-2/3 SSH biases having applied ECMWF-based ZWDs to the Jason-2/3 ranges, and found that the mean Jason-2 and Jason-3 SSH biases increased by 18 mm and 12 mm respectively to +2 mm and −11 mm respectively, compared with −16 mm and −23 mm respectively on applying the MWR-based ZWDs. These respective 18 mm and 12 mm SSH increases arise because the ECMWF-based ZWDs are consistently greater than the MWR-based ZWDs (see Table III) by 17 mm and 11 mm for Jason-2 and Jason-3, respectively. Hence shorter corrected ranges arise when applying ECMWF values over MWR values, although it should be noted that the sample size here is small. Regardless of the tropospheric correction method, the individual Jason-2/3 altimetry and GNSS WG SSH agreements (biases) all range from +12 mm to −40 mm, which are almost within the bounds of the cal/val biases described in Section IV for previous Jason-2/3 studies in other geographical regions. Similarly, the CryoSat-2 SSH biases on applying GPD+ ZWDs are +18 mm and −29 mm, which are commensurate with those found in other geographical regions.

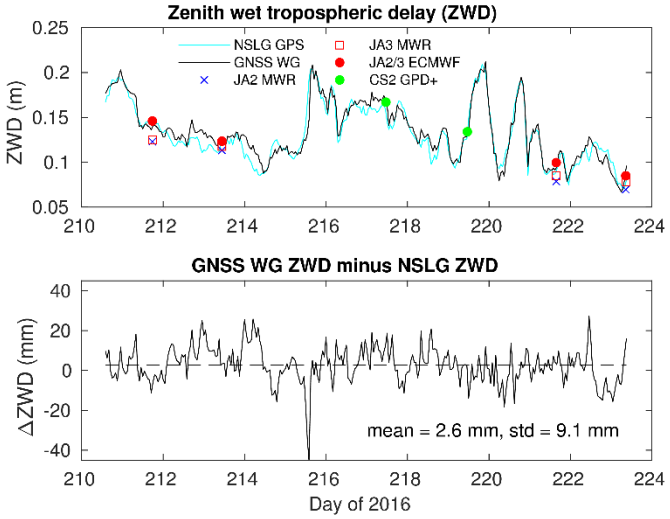

Fig. 4. Zenith wet tropospheric delays (ZWDs) estimated at the GNSS WG and NSLG onshore static GPS reference station (black and cyan lines respectively, upper pane), together with their differences (lower pane). Also shown in the upper pane are the altimetry MWR-based ZWDs for Jason-2 (blue crosses) and Jason-3 (unfilled red squares) and ECMWF-based ZWDs for Jason-2/3 (red circles) and GPD+ ZWDs for CryoSat-2 (green circles). The values of the differences between the MWR-based ZWDs and the GNSS WG estimated ZWDs are listed in Table III, together with the ECMWF minus GNSS WG ZWD differences.

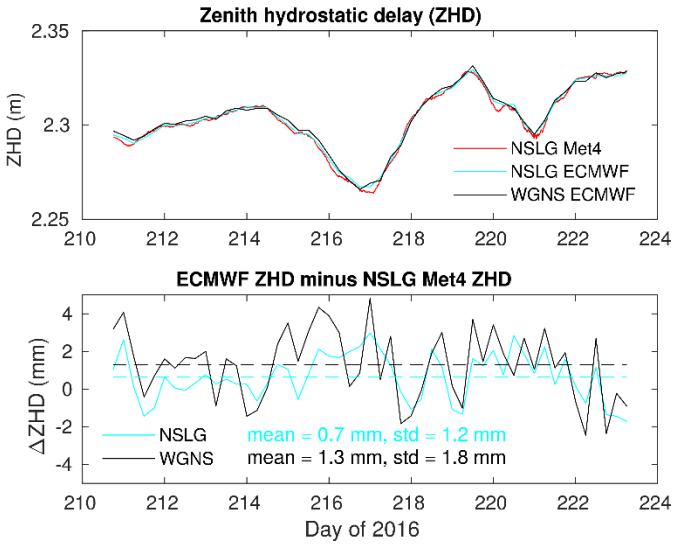

Fig. 5. Zenith hydrostatic delay (ZHD) (upper pane) and arising differences (lower pane) computed for the NSLG onshore static GNSS reference station using pressure from the ECMWF model (6-hourly) according to [82] and observed by a Paroscientific Met4 sensor (every 5 min).

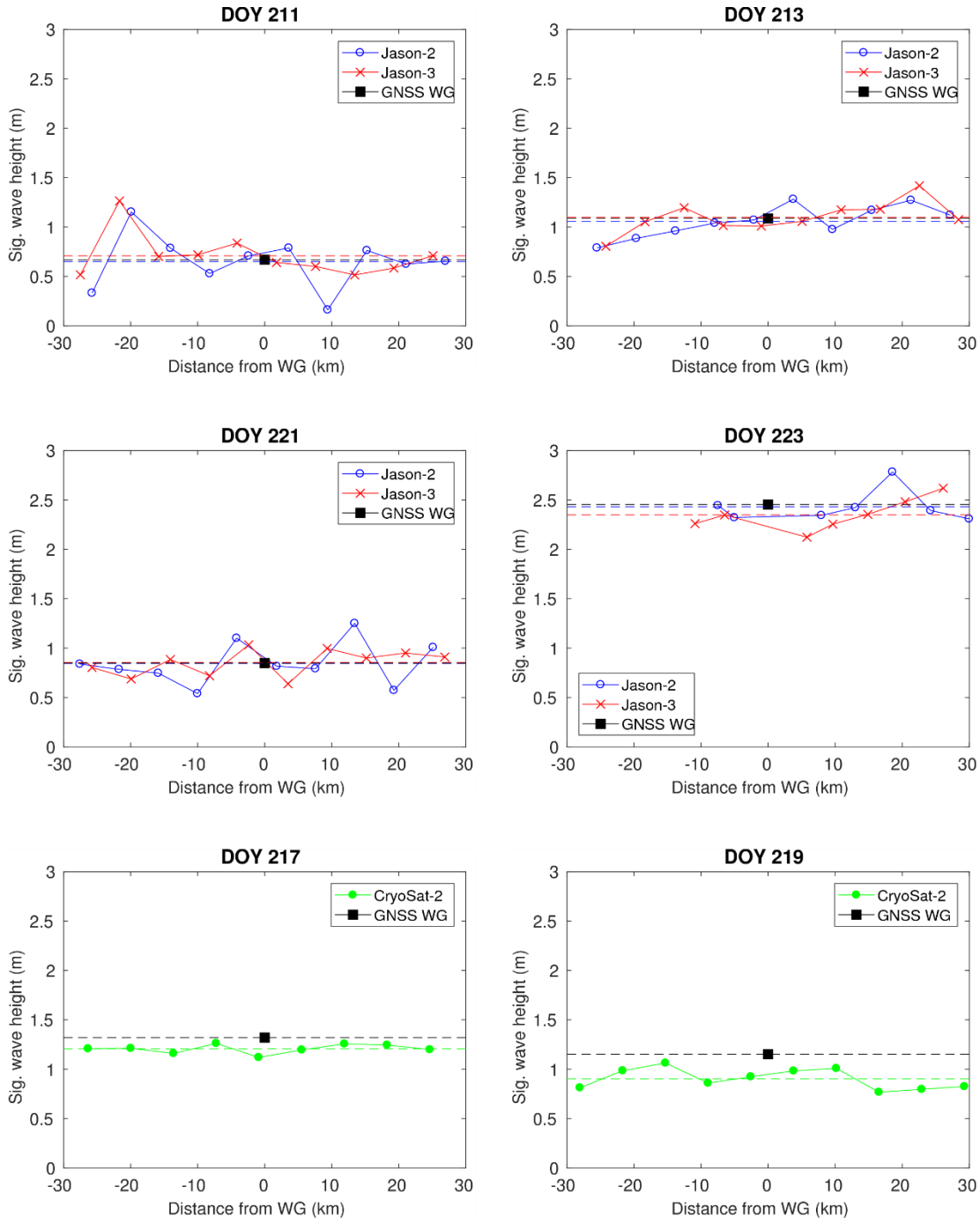

Fig. 6. Significant wave height (SWH) obtained from Jason-2/3 1 Hz measurements within ±30 km of the GNSS Wave Glider (GNSS WG) and at least 9.5 km from land on day of year (DOY) 211, 213, 221 and 223 (upper and middle panes). The dashed blue and red lines denote the mean of the Jason-2 and Jason-3 SWHs at the 1 Hz points. The black square shows the SWH measured by the GNSS WG, computed using 2 minutes of 5 Hz wave heights, centered about the mid-epoch of the Jason-2/3 overpasses. The lower two panes represent the equivalent plots for CryoSat-2 on DOY 217 and 219. Satellite approach distances from the WG are denoted as negative, departure distances as positive.

TABLE IV

SIGNIFICANT WAVE HEIGHT (SWH) DIFFERENCES BETWEEN THE GNSS WG AND JASON-2 (JA2), JASON-3 (JA3) AND CRYOSAT-2 (CS2) ALTIMETRY SATELLITES USING 1 HZ GDR/GOPR PRODUCTS. THE DIFFERENCES ARE SHOWN FOR BOTH THE SINGLE 1 HZ DATA POINT NEAREST THE WG, AND ALSO FROM THE AVERAGE MEASURED BY ALL 1 HZ DATA POINTS WITHIN ±30 KM OF THE WG. 'DOY' DENOTES THE DAY OF YEAR (2016) OF THE ASSOCIATED SWH VALUES. VALUES ARE LISTED IN CENTIMETERS.

		DOY 211	DOY 213	DOY 217	DOY 219	DOY 221	DOY 223	RMS
Nearest altim minus GNSS	**JA2**	4	−2			−3	−13	7
	JA3	−3	−8			18	−33	19
	CS2			−20	−23			22
Ave altim minus GNSS	**JA2**	−2±3	−3±2			0±2	−2±2	2
	JA3	4±2	1±2			0±1	−11±2	6
	CS2			−11±1	−25±1			19

C. Significant Wave Height Validation

The Jason-2/3 1 Hz SWH measurements for each of their four passes are shown in Fig. 6, along with those from the two CryoSat-2 passes, and the GNSS WG SWH measurement per pass is also plotted. In the small sample size considered, there is more scatter in the Jason SWH estimates than in those from CryoSat-2, but when averaged, the agreements with the GNSS WG are closer for Jason than CryoSat-2. As listed in Table IV, the RMS of the average agreements among the four Jason passes is only 2 cm and 6 cm for Jason-2 and Jason-3 respectively, while for CryoSat-2 the RMS of the average agreements is 19 cm. These are at least commensurate with previous altimetry SWH cal/val studies with wave buoys such as [46] and [47], and the small differences for Jason in particular illustrate the suitability of the GNSS WG for altimetry SWH measurement cal/val. If only the 1 Hz altimetry SWH measurement nearest the GNSS WG is used per pass (values listed in Table IV), the RMS agreements are 7 cm and 19 cm for Jason-2 and Jason-3 respectively, larger than the respective 2 cm and 6 cm averages, illustrating the need to take averages of multiple measurements when the Jason satellites pass over the GNSS WG. For CryoSat-2, the RMS of the differences between the nearest altimetry SWH measurements and the GNSS WG SWHs is 22 cm.

VII. CONCLUSION

We have demonstrated that an unmanned surface vehicle, the GNSS Wave Glider, is capable of providing absolute cal/val of altimetry satellite measurements of sea surface height for multiple passes of multiple satellites (Jason-2, Jason-3 and CryoSat-2) at different locations over the same region (here the North Sea). Our results demonstrate the concept of the GNSS WG as an additional, versatile platform for altimetry satellite SSH cal/val, not withstanding our small sample size considered and the fairly benign sea conditions (SWH up to 2.5 m, wind gust speeds up to 15 m/s) under which our results were obtained. The GNSS WG has the advantage over cal/val proposals such as the towed carpet of [17] that no support vessel is needed (although regular, but not necessarily frequent, web-based human pilot checks are needed) and it provides an absolute, in-situ measurement. Hence no extrapolation of geoid, tide or dynamic topography models from the coastline is undertaken as is needed for indirect coastal tide gauge cal/val approaches. The GNSS WG has all the capabilities of a GNSS buoy (it can readily operate in a holding location by being set to navigate continuously around an area of only a few hundred meters), but has the advantage over GNSS buoys in that it is not constrained to a single location, can be used for multiple satellites and tracks, without the need for expensive and logistically challenging redeployment and recovery. The GNSS WG may also be deployed and piloted equally readily either over shallow, coastal seas or the deep ocean. The only restrictions are a 10 m minimum water depth requirement and the need for sufficient incoming shortwave solar radiation to ensure sufficient power for continuous operation of the onboard instrumentation, which can be satisfied from about March to September for mid-latitudes in the northern hemisphere.

Similar cal/val altimetry minus GNSS SSH differences have been obtained with the GNSS Wave Glider in the North Sea (a region which has not had such absolute GNSS cal/val experiments reported to date) to those in previous cal/val experiments at other geographical locations that used either GPS buoys or static GPS reference stations. Using 20 Hz altimetry data within ±30 km of the GNSS WG in the North Sea, Jason-2 biases of −30 to −8 mm were obtained from four passes in July-August 2016, and Jason-3 biases of −40 to +1 mm for the same four passes. The Jason-2 SSH was found to be on average 7 mm higher than Jason-3 SSH. These SSH biases are almost commensurate with the −30 to +30 mm Jason-2/3 values found in previous studies for other parts of the world, such as both the western and eastern parts of the Mediterranean Sea, the eastern Pacific Ocean and the Bass Strait. However, we see a reduction in the difference between Jason-2 and Jason-3 compared with systematic Jason-2 minus Jason-3 differences of 30 mm previously found, possibly because we used the more recent GDR-F product for Jason-3 (there was no GDR-F product available for Jason-2, only the older GDR-D product which we used). For CryoSat-2, we obtained SSH biases of −29 mm and +18 mm for the two respective ascending passes using the GOPR baseline C product. These biases are at least commensurate with the biases of +83 to −12 mm for the German Bight implied by [37], although they are larger than the 5-8 mm biases around Corsica reported by [13]. Our Jason results were based on using altimetry data, including microwave radiometer wet delay corrections, up to 9.5 km from land. For CryoSat-2, ECMWF-based tropospheric corrections were used, and the

distance from land was always more than 27 km. It should be noted that our absolute biases are determined from a very small sample and we have not yet undertaken a comprehensive laboratory, harbor or sea-based experiment to rigorously determine the GNSS antenna to sea surface offset. The exact value of the offset to be applied will also likely vary in accordance with the dynamic response of the WG to the waves and water velocity, with tilt likely increasing with increasing SWH and this, together with water velocity impact, will need thorough investigation, likely including with INS measurements.

We showed that the GNSS measurements from the Wave Glider processed in kinematic precise point positioning mode provided hourly zenith wet tropospheric delay estimates which agreed with those from a nearby coastal static GPS receiver (NSLG) with a mean difference of 2.6 mm and a difference standard deviation of 9.1 mm. Therefore, they furnished a means of cal/val of the wet delay measured by the Jason-2/3 onboard microwave radiometer and applied in the Jason-2/3 altimetry data processing, the alternative ECMWF modeled tropospheric delays, and the GPD+ tropospheric model used in the CryoSat-2 altimetry processing. The MWR-based ZWDs used here were always shorter than the GNSS WG ZWDs, with mean (MWR-GNSS) differences of −15 mm for Jason-2 and −10 mm for Jason-3, which was not substantially affected by the distance from the coast (23-64 km). For Jason-2/3, the ECMWF-based modeled ZWDs were found to be −5 to +7 mm different from the GNSS-estimated ZWDs. If these ECMWF-based ZWDs were applied in the altimetry processing, the mean sea surface height increased by 18 mm and 12 mm for Jason-2 and Jason-3 respectively compared with when applying radiometer measured delays, with the mean Jason-2 minus GNSS SSH bias increasing from −16 to +2 mm, and that for Jason-3 increasing from −23 to −11 mm. All individual sea surface height Jason-2/3 biases were within the range of −40 to +12 mm irrespective of whether MWR or ECMWF model tropospheric corrections were applied. For CryoSat-2, the ECMWF/GPD+ modeled ZWDs were found to be 3-5 mm different from the GNSS WG ZWDs.

Significant wave height (SWH) measurements from all of Jason-2/3 and CryoSat-2 1 Hz products were compared with those from the GNSS WG, with RMS agreements of 2 and 6 cm obtained for Jason-2 and Jason-3 respectively, and agreements of 19-22 cm for CryoSat-2, demonstrating the suitability of the GNSS WG for SWH cal/val, as well as SSH and ZWD.

While we have focused here on demonstrating the capability of GNSS WGs as mobile platforms for the cal/val of altimetry measurements, the close agreement between the data collected by these two means, suggests, in turn, that GNSS WGs can be reliably used to carry out surveys of the state of the sea surface at temporal and spatial scales that are not well resolved by satellite-based observing systems. Notable such scenarios arise near coastlines, where precise altimetry encounters difficulties due to land contamination of the radar signals, and also in remote, high latitude areas.

Acknowledgment

Thanks to the following for the free provision of data/products: Geoff Blewitt for making Gipsy-X tropospheric delays available (http://geodesy.unr.edu/); NASA JPL for the GipsyX software, orbits and clock products; NERC BIGF for the MORO GNSS data; AVISO for providing the Jason-2/3 geophysical data records; ESA for providing the CryoSat-2 geophysical ocean products; NGA for the EGM2008 geoid model; DGFI-TUM for the EOT20 ocean tide model. The raw GNSS data from the Wave Glider are available at doi:10.5281/zenodo.1250342. Thanks also to Liam Rogerson for help with piloting, and Neil Armstrong and Barry Pearson (crew of The Princess Royal) for their field assistance in the deployment and recovery of the Wave Glider. Careful reviews by Christopher Watson and an anonymous reviewer are acknowledged.

References

[1] International Altimetry team, “Altimetry for the future: Building on 25 years of progress,” *Advances in Space Research*, 68(2), 319-363, 2021.

[2] M. Ablain et al.,“Improved sea level record over the satellite altimetry era (1993-2010) from the Climate Change Initiative project,” *Ocean Science*, 11, 67-82, 2015.

[3] X. Dong, P. Woodworth, P. Moore, and R. Bingley, “Absolute calibration of the TOPEX/POSEIDON altimeters using UK tide gauges, GPS, and precise, local geoid-differences,” *Marine Geodesy*, 25(3), 189-204, 2002.

[4] C. Watson, R. Coleman, N. White, J. Church, and R. Govind, “Absolute calibration of TOPEX/Poseidon and Jason-1 using GPS buoys in Bass Strait, Australia,” *Marine Geodesy*, 26, 285-304, 2003.

[5] C. M. Murphy, P. Moore, and P. Woodworth, “Short-arc calibration of the TOPEX/POSEIDON and ERS 1 altimeters utilizing in situ data,” *Journal of Geophysical Research*, 101(C6), 14,191-14,200, 1996.

[6] P. Woodworth, P. Moore, X. Dong, and R. Bingley, “Absolute calibration of the Jason-1 altimeter using UK tide gauges,” *Marine Geodesy*, 27(1-2), 95-106, 2004.

[7] G. T. Mitchum, “An improved calibration of satellite altimetric heights using tide gauge sea levels with adjustment for land motion,” *Marine Geodesy*, 23, 145-166, 2000.

[8] P. Bonnefond, B. J. Haines, and C. Watson, “In situ absolute calibration and validation: A link from coastal to open-ocean altimetry,” *Coastal Altimetry* (Spinger, ed. S. Vignudelli et al), 259-296, 2011.

[9] G. Piccioni, D. Dettmering, M. Passaro, C. Schwatke, W. Bosch, and F. Seitz, “Coastal improvements for tide models: The impact of ALES retracker,” *Remote Sensing*, 10(700), 2018.

[10] R. J. Bingham, K. Haines, and C. W. Hughes, “Calculating the ocean’s mean dynamic topography from a mean sea surface and a geoid,” *Journal of Atmospheric and Oceanic Technology*, 25(10), 1808-1822, 2008.

[11] J. Huang, “Determining coastal mean dynamic topography by geodetic methods,” *Geophysical Research Letters*, 44, 11125–11128, 2017.

[12] B. Haines, S. D. Desai, D. Kubitschek, and R. R. Leben, “A brief history of the Harvest experiment: 1989-2019,” *Advances in Space Research*, 68(2), 1161-1170, 2021.

[13] P. Bonnefond, P. Exertier, O. Laurain, T. Guinle, and P. Féménias, “Corsica: A 20-yr multi-mission absolute altimeter calibration site,” *Advances in Space Research*, 68, 1171-1186, 2021.

[14] X. Deng and W. E. Featherstone, “A coastal retracking system for satellite radar altimeter waveforms: Application to ERS-2 around Australia,” *Journal of Geophysical Research*, 111, C06012, 2006.

[15] E. Obligis, C. Desportes, L. Eymard, M. J. Fernandes, C. Lázaro, and A. L. Nunes, “Tropospheric corrections for coastal altimetry,” In Vignudelli et al. (Eds.), *Coastal Altimetry*, Springer-Verlag, Chapter 6, 147-176, 2011.

[16] B. Zhou, C. Watson, J. Beardsley, B. Legresy, and M. A. King, “Development of a GNSS/INS buoy array in preparation for SWOT validation in Bass Strait,” *Frontiers in Marine Science*, 9:1093391, doi: 10.3389/fmars.2022.1093391, 2023.

[17] C. Chupin, V. Ballu, L. Testut, Y.-T. Tranchant, M. Calzas, E. Poirier, T. Coulombier, O' Laurain, P. Bonnefond, and Team FOAM Project, "Mapping sea surace height using new concepts of kinematic GNSS instruments," *Remote Sensing*, 12, 2656, doi:10.3390/rs12162656, 2020.

[18] P. Bonnefond, O. Laurain, P. Exertier, M. Calzas, T. Guinle, N. Picot, and the FOAM Project Team, "Validating a new GNSS-based sea level instrument (CalNaGeo) at Senetosa Cape", *Marine Geodesy*, 45(2), 121-150, 2022.

[19] N. T. Penna, M. A. Morales Maqueda, I. Martin, J. Guo, and P. R. Foden, "Sea surface height measurement using a GNSS Wave Glider," *Geophysical Research Letters*, 45, 2018.

[20] T. Daniel, J. Manley, and N. Trenaman, "The Wave Glider: Enabling a new approach to persistent ocean observation and research," *Ocean Dynamics*, 61, 1509-1520, 2011.

[21] M. A. Morales Maqueda, N. T. Penna, S. D. P. Williams, P. R. Foden, I. Martin, and J. Pugh, "Water surface height determination with a GPS Wave Glider: A demonstration in Loch Ness, Scotland," *Journal of Atmospheric and Oceanic Technology*, 33(6), 1159-1168, 2016.

[22] D. B. Chelton, J. C. Ries, B. J. Haines, L.-L. Fu, and P. S. Callahan, "Satellite altimetry," In L.-L. Fu and A. Cazanave (eds.), *Satellite altimetry and Earth science, International Geophysics Series*, 69(1), 1-131, CA: Academic Press, 2001.

[23] OSTM, "OSTM/Jason-2 Products Handbook," *1*(11), 13 January 2017, https://www.ospo.noaa.gov/Products/documents/hdbk_j2.pdf, 2017.

[24] L. Yang, X. Zhou, S. P. Mertikas, L. Zhu, L. Yang, and N. Lei, "First calibration results of Jason-2 and SARAL/AltiKa satellite altimeters from the Qianli Yan permanent Cal/Val facilities, China," *Advances in Space Research*, 59, 2831-2842, 2017.

[25] S. P. Mertikas et al., "Fifteen years of cal/val service to reference altimetry missions: Calibration of satellite altimetry at the permanent facilities in Gavdos and Crete, Greece," *Remote Sensing*, 10, 1557, 2018.

[26] F. Frappart et al., "The 2013 Ibiza calibration campaign of Jason-2 and SARAL altimeters," *Marine Geodesy*, 38(S1), 219-232, 2015.

[27] B. J. Haines, S. D. Desai, and G. H. Born, "The Harvest experiment calibration of the climate data record from TOPEX/Poseidon, Jason-1 and the Ocean Surface Topography Mission," *Marine Geodesy*, 33(S1), 91-113, 2010.

[28] P. Bonnefond, P. Exertier, O. Laurain, and G. Jan, "Absolute calibration of Jason-1 and Jason-2 altimeters in Corsica during the formation flight phase," *Marine Geodesy*, 33(S1), 80-90, 2010.

[29] C. Watson, N. White, J. Church, R. Burgette, P. Tregoning, and R. Coleman, "Absolute calibration in Bass Strait, Australia: TOPEX, Jason-1 and OSTM/Jason-2," *Marine Geodesy*, 34(3-4), 242-260, 2011.

[30] S. P. Mertikas et al., "Statistical models and latest results in the determination of the absolute bias for the radar altimeters of Jason satellites using the Gavdos facility," *Marine Geodesy*, 33(S1), 114-149, 2010.

[31] K.-C. Cheng, C.-Y. Kuo, H.-Z. Tseng, Y. Yi, and C. K. Shum, "Lake surface height calibration of Jason-1 and Jason-2 over the Great Lakes," *Marine Geodesy*, 33(S1), 186-203, 2010.

[32] J.-F. Crétaux et al., "Absolute calibration of Jason radar altimeters from GPS kinematic campaigns over Lake Issykkul," *Marine Geodesy*, 34(3-4), 291-318, 2011.

[33] J.-F. Crétaux et al., "Absolute calibration or validation of the altimeters on the Sentinel-3A and the Jason-3 over Lake Issykkul (Kyrgyzstan)," *Remote Sensing*, 10, 1679, 2018.

[34] W. Zhai, J. Zhu, X. Fam, L. Yan, C. Chen, and Z. Tian, "Preliminary calibration results for Jason-3 and Sentinel-3 altimeters in the Wanshan Islands," *Journal of Oceanology and Limnology*, 39(2), 458-471, 2021.

[35] L. Yang et al., "Monitoring the performance of HY-2B and Jason-2/3 sea surface height via the China Altimetry Calibration Cooperation Plan," *IEEE Transactions on Geoscience and Remote Sensing*, 60, 1002013, 2022.

[36] C. Chupin, V. Ballu, L. Testut, Y.Y. Tranchant, and J. Aucan, "Nouméa: A new multi-mission calibration and validation site for past and future altimetry missions?," *Ocean Science*, 19, 1277-1314, 2023.

[37] L. Fenoglio-Marc et al., "The German Bight: A validation of CryoSat-2 altimeter data in SAR mode," *Advances in Space Research*, 55, 2641-2656, 2015.

[38] P. Bonnefond et al., "Calibrating the SAR SSH of Sentinel-3A and CryoSat-2 over the Corsica Facilities," *Remote Sensing*, 10(92), 2018.

[39] A. Sibthorpe, S. Brown, S. D. Desai, and B. J. Haines, "Calibration and validation of the Jason-2/OSTM advanced microwave radiometer using terrestrial GPS stations," *Marine Geodesy*, 34, 420-430, 2011.

[40] W. Zhai, J. Zhu, C. Chen, H. Wang, X. Huang, and L. Yan, "The validation of wet zenith delay of ground GPS stations based on Jason-2 AMR," *IGARSS 2018 IEEE International Geoscience and Remote Sensing Symposium*, Valencia, Spain, 7628-7631, 2018.

[41] W. Zhai et al., "GNSS data processing and validation of the altimeter zenith wet delay around the Wanshan calibration site," *Remote Sensing*, 14, 6235, 2022.

[42] L. Zhu, L. Yang, Y. Xu, H. Zhang, Z. Wu, and Z. Wang, "Independent Validation of Jason-2/3 and HY-2B microwave radiometers using Chinese coastal GNSS," *IEEE Transactions on Geoscience and Remote Sensing*, 60, 1–11, 2022.

[43] T. Vieira, M. J. Fernandes, and C. Lázaro, "Independent assessment of on-board microwave radiometer measurements in coastal zones using tropospheric delays from GNSS," *IEEE Transactions on Geoscience and Remote Sensing*, 57(3), 1804-1816, 2019.

[44] C. Pearson, P. Moore, and S. Edwards, "GNSS assessment of sentinel-3A ECMWF tropospheric delays over inland waters," *Advances in Space Research*, 66, 2827-2843, 2020.

[45] M. J. Fernandes and C. Lázaro, "GPD+ wet tropospheric corrections for CryoSat-2 and GFO altimetry missions," *Remote Sensing*, 8(10), 851, 2016.

[46] R. D. Ray and B. D. Beckley, "Calibration of ocean wave measurements by the TOPEX, Jason-1 and Jason-2 satellites," *Marine Geodesy*, 35, 238-257, 2012.

[47] J. Yang, J. Zhang, Y. Jia, C. Fan, and W. Cui, "Validation of Sentinel-3A/3B and Jason-3 altimeter wind speeds and significant wave heights using buoy and ASCAT data," *Remote Sensing*, 12(13), 2079, 2020.

[48] M. Passaro, L. Fenoglio-Marc, and P. Cipollini, "Validation of significant wave height from improved satellite altimetry in the German Bight," *IEEE Transactions on Geoscience and Remote Sensing*, 53(4), 2015.

[49] S. Abdalla, S. Dinardo, J. Benveniste, and P. A. E. M. Janssen, "Assessment of CryoSat-2 SAR mode wind and wave data," *Advances in Space Research*, 62, 1421-1433, 2018.

[50] G. Petit and B. Luzum, "IERS Conventions (2010)," *IERS Technical Note 36*, 2010.

[51] J. Boehm, A. Niell, P. Tregoning, and H. Schuh, "Global Mapping Function (GMF): A new empirical mapping function based on numerical weather model data," *Geophysical Research Letters*, 33, L07304, 2006a.

[52] B. Zhou, C. Watson, B. Legresy, M. A. King, J. Beardsley, and A. Deane, "GNSS/INS-equipped buoys for altimetry validation: Lessons learnt and new directions from the Bass Strait validation facility," *Remote Sensing*, 12, 3001, 2020.

[53] B. Zhou, C. Watson, B. Legresy, M. A. King, and J. Beardsley, "Ongoing developments of the Bass Strait GNSS/INS buoy system for altimetry validation in preparation for SWOT," *Remote Sensing*, 15(1), 287, 2023.

[54] Haines, B., S. Desai, C. Meinig, and S. Stalin, "CALVAL of the SWOT SSH spectrum: Moored GPS buoy approach," *SWOT Second Science Team Meeting*, Toulouse, France, NASA, 11 pp., https://hdl.handle.net/2014/48164, 2017.

[55] T. Kato, Y. Terada, K. Tadokoro, and A. Futamura, "Developments of GNSS buoy for a synthetic geohazard monitoring system," *Proceedings of the Japan Academy, Series B Physical and Biological Sciences*, 98(2), 49-71, 2022.

[56] G. Liang, S. Li, K. Bao, G. Wang, F. Teng, F. Zhang, Y. Wang, S. Guan, and Z. Wei, "Development of GNSS Buoy for Sea Surface Elevation Observation of Offshore Wind Farm," *Remote Sensing*, 15, 5323. https://doi.org/10.3390/rs15225323, 2023.

[57] S. Fan, Y. Liu, C. Xu, J. Guo, and Z. Wang, "GPS kinematic precise point positioning based on sequential least squares estimation," *18th International Conference on Geoinformatics*, Beijing, China, pp. 1-5, doi: 10.1109/GEOINFORMATICS.2010.5567623, 2010.

[58] C. De Marez, J. Callies, B. Haines, D. Rodriguez-Chavez, and J. Wang, "Observational constraints on the submesoscale sea surface height variance of balanced motion," *Journal of Physical Oceanography*, 53(5), 1221-1235, 2023.

[59] F. Fund, F. Perosanz, L. Testut, and S. Loyer, "An integer precise point positioning technique for sea surface observations using a GPS buoy,", *Advances in Space Research*, 51, 1311-1322, 2013.

[60] N. T. Penna, P. J. Clarke, M. S. Bos, and T. F. Baker, Ocean tide loading displacements in western Europe: 1. Validation of kinematic GPS estimates, *Journal of Geophysical Research: Solid Earth*, 120(9), 6540-6557, 2015.

[61] N. T. Penna, A. H. Dodson, and W. Chen, "Assessment of EGNOS tropospheric correction model," *Journal of Navigation*, 54(1), 37-55, 2001.

[62] F. K. Brunner, and W. M. Welsch, "Effect of the troposphere on GPS measurements," GPS World, January 1993, 42-51, 1993.

[63] M. Abbaszadeh, P. J. Clarke, and N. T. Penna, "Benefits of combining GPS and GLONASS for measuring ocean tide loading displacement," *Journal of Geodesy*, 94(63), 2020.

[64] B. Grayson, N. T. Penna, J. P. Mills, and D. S. Grant, "GPS precise point positioning for UAV photogrammetry," *Photogrammetric Record*, 33(164), 427-447, 2018.

[65] S. Erol, "A comparative study for performance analysis of kinematic mult-constellation gnss ppp in dynamic environment," *Journal of Marine Science and Engineering*, 8(7), 1-19, 2020.

[66] M. Gurturk, and M. Soycan, "Accuracy assessment of kinematic PPP versus PPK for GNSS flights data processing," *Survey Review*, 54(382), 48-56., 2022.

[67] F. Mertz, J. P. Dumont, and S. Urien, "Baseline-C CryoSat ocean processor ocean product handbook,", European Space Agency, v4.1, https://earth.esa.int/eogateway/documents/20142/37627/CryoSat-Baseline-C-Ocean-Product-Handbook.pdf/d4718bd4-65ae-20a6-5ea9-ee3cde121f7c , 2019.

[68] P. Wessel, W.H.F. Smith, R. Scharoo, J. Luis, and F. Wobbe, "Generic Mapping Tools: Improved version release," *EoS Transactions American Geophysical Union*, 94(45), 409-410, 2013.

[69] S. Vignudelli et al., "Satellite altimetry measurements of sea level in the coastal zone," *Surveys in Geophysics*, 40, 1319-1349, 2019.

[70] S. Brown, "A novel near-land radiometer wet path-delay retrieval algorithm: Application to the Jason-2/OSTM Advanced Microwave Radiometer," *IEEE Transactions on Geoscience and Remote Sensing*, 48(4), 1986-1992, 2010.

[71] Jason-3, "Jason-3 Products Handbook," 1(5), 17 September 2018, https://www.ospo.noaa.gov/Products/documents/hdbk_j3.pdf, 2018.

[72] P. D. Cotton et al., "Improved oceanographic measurements with CryoSat SAR altimetry: Results and roadmap from ESA CryoSat Plus for Oceans Project," *Proceedings of the ESA Living Planet Symposium*, 9-13 May 2016, Prague, Czech Republic, ESA Special Publication SP-740 (CD-ROM). http://www.satoc.eu/projects/CP4O/docs/0519cotton%20_CP4Oroadmap.pdf, 2016.

[73] N. K. Pavlis, S. A. Holmes, S. C. Kenyon, and J. K. Factor, "The development and evaluation of the Earth Gravitational Model 2008 (EGM2008)," *Journal of Geophysical Research*, 117, B04406, 2012.

[74] N. K. Pavlis, S. A. Holmes, S. C. Kenyon, and J. K. Factor, Correction to "The development and evaluation of the Earth Gravitational Model 2008 (EGM2008)," *Journal of Geophysical Research: Solid Earth*, 118, 2633, 2013.

[75] M. G. Hart-Davis, G. Piccioni, D. Dettmering, C. Schwatke, M. Passaro, and F. Seitz, "EOT20: a global ocean tide model from multi-mission satellite altimetry," *Earth System Science Data*, 13, 3869-3884, 2021.

[76] L. Carrère and F. Lyard, "Modeling the barotropic response of the global ocean to atmospheric wind and pressure forcing – comparisons with observations," *Geophysical Research Letters*, 30, 1275, 2003.

[77] P. Thibaut, J. C. Poisson, E. Bronner, and N. Picot, "Relative performance of the MLE3 and MLE4 retracking algorithms on Jason-2 altimeter waveforms," *Marine Geodesy*, 33, 217-335, 2010.

[78] D. E. Cartwright and A. C. Edden, "Corrected tables of tidal harmonics," *Geophysical Journal of the Royal Astronomical Society*, 33, 253-264, 1973.

[79] Z. Altamimi, P. Rebischung, L. Métivier, and X. Collilieux, "ITRF2014: A new release of the International Terrestrial Reference Frame modeling non-linear station motions," *Journal of Geophysical Research Solid Earth*, 121, 6109-6131.

[80] J. Guo, H. Zhang, Z. Li, C. Zhu, and X. Liu, "On modelling sea state bias of Jason-2 altimeter data based on significant wave heights and wind speeds," *Remote Sensing*, 15, 2666, 2023.

[81] G. Blewitt, W. C. Hammond, and C. Kreemer, "Harnessing the GPS data explosion for interdisciplinary science," *Eos*, 99, 2018.

[82] J. Boehm, B. Werl, and H. Schuh, "Troposphere mapping functions for GPS and very long baseline interferometry from European Centre for Medium-Range Weather Forecasts operational analysis data," *Journal of Geophysical Research: Solid Earth*, 111(B02406), 2006b.

[83] J. L. Davis, T. A. Herring, I. I. Shapiro, A. E. E. Rogers, and G. Elgered, "Geodesy by radio interferometry: Effects of atmospheric modeling errors on estimates of baseline length," *Radio Science*, 20(6), 1593-1607, 1985.

[84] Y. Gong and Z. Liu, "Evaluating the accuracy of Jason-3 water vapor product using PWV data from global radiosonde and GNSS stations," *IEEE Transactions on Geoscience and Remote Sensing*, 59(5), 4008-4017, 2021.